

SIMULATION OF OPTICAL REMOTE SENSING SYSTEMS FOR EARTH RESOURCE ANALYSIS¹

J P Kerekes & D A Landgrebe

Laboratory for Applications of Remote Sensing
and School of Electrical Engineering
Purdue University, West Lafayette, Indiana, USA

ABSTRACT

A system model for the simulation of remote sensing systems is presented. The system is seen to be divided into three parts: the scene, the sensor, and the processing algorithms. Models are presented for these various component systems. Results of the simulation for various scene and sensor configurations are included.

Keywords: Remote Sensing System, Simulation, Models

1. INTRODUCTION

As both sensor systems and processing systems become increasingly complex, the need increases for understanding the impact of various system parameters on system performance. In many remote sensing systems, the design of the sensor and of processing algorithms has been done in an ad hoc manner, often relying on the experience, or judgement, of the designers. This was necessary because of the vast complexity of even the most simple systems. Also because of this complexity, various parts of the system were designed by experts in those areas, often without consideration to the rest of the system. But now, as our understanding of these various parts of the system

increases, and the computational power available grows, it is becoming feasible to investigate the design of remote sensing systems using accurate computational models. A study of particular sensor configurations and processing algorithms presented in (Ref. 1) used this approach.

In this paper we present an attempt at modeling remote sensing systems with the goal being an increased understanding of the interrelated effects of system parameters. In the next section we discuss the scope of the system and present the overall system model. This is followed by discussions of the models for the various parts of the system, including the definition and the parameters of each model. Finally, initial results of applying the model to various system configurations are presented to show how the simulation can be used to investigate the interrelated effects of system parameters.

2. REMOTE SENSING SYSTEM MODEL

The research has centered around passive optical sensors (airborne or spaceborne) used in Earth resource analysis applications. Examples of these include the SPOT and Landsat sensor systems. Figure 1 shows the overall structure of the remote sensing system model used. This division of the system was

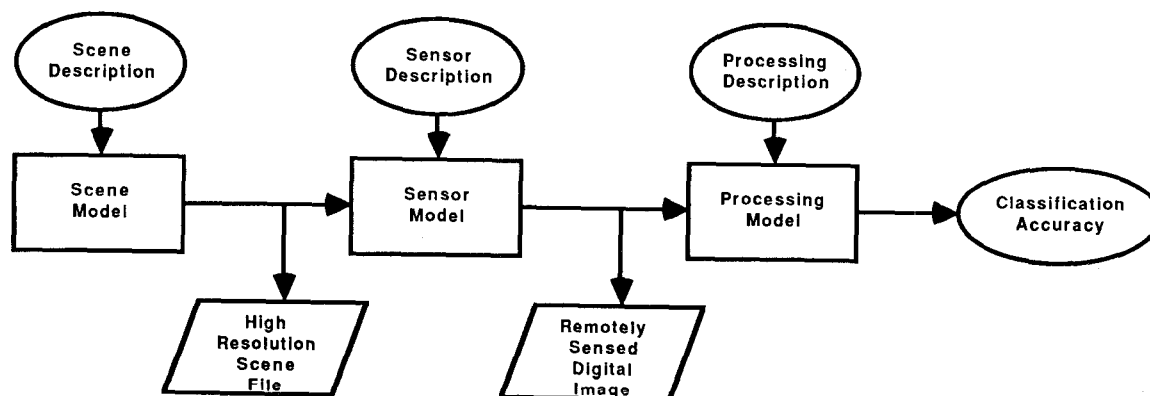


Figure 1. Remote Sensing System Model

¹ The work reported in this paper was funded in part by NSF Grant ECS 8507405

described in our previous work (Ref. 2), and was chosen to allow both fidelity and flexibility in the system simulation. Scene models can be chosen appropriately for various types of scenes to be used, with a common interface to the sensor being a high resolution scene file. This file contains a high resolution discrete version of the spectral radiance function present at the input aperture of the sensor. A user defined sensor then uses this scene file to create a remotely sensed multispectral image. Specified processing algorithms are then applied to this multispectral image to obtain a resultant classification accuracy.

3. SCENE MODEL

The task of the scene model is to accept a description of the scene and produce a high spatial and spectral resolution scene file consisting of the spectral radiance seen by the sensor. By high spatial resolution, we mean scene pixel sizes several times smaller than those of the sensor. High spectral resolution means several spectral samples per sensor spectral band.

The form of the scene model we have chosen combines a stochastic surface reflectance model with a deterministic solar and atmospheric model. For each scene pixel in a user defined class area a mean reflectance vector has added to it a standard deviation vector multiplied by a Gaussian random variable. The random variables are arranged in a spatially correlated manner according to a 2-D autoregressive model. The atmospheric simulation program LOWTRAN (Ref. 3) computes the solar irradiance, skylight radiance, atmospheric transmittance and scattered path radiance to complete the scene model. The following table shows the user defined parameters for the scene model.

<u>Scene Parameters</u>	<u>Symbol</u>
Number of scene classes	K
Mean reflectance (class k)	$\rho_k(\lambda)$
Std. deviation of reflectance	$\sigma_k(\lambda)$
Boundaries (class k)	B_k
Wavelength range, increment	$\Lambda, \Delta\lambda$
Scene size	I cols by J rows
Ground size of scene pixel	G
Atmospheric type	a
Meteorological range	V_η
Solar zenith angle	θ_{sun}
Solar azimuth angle	ϕ_{sun}
Sensor zenith angle	θ_{sensor}
Sensor azimuth angle	ϕ_{sensor}
Spatial model parameters	C_1, C_2, C_3, σ_u

Table 1. Scene Model Parameters

The spectral radiance present at the input of the sensor is obtained in the following manner. First, a two dimensional array of Gaussian random numbers, $s(i,j)$, is generated according to Eq. 1,

$$s(i,j) = C_1s(i-1,j) + C_2s(i,j-1) + C_3s(i-1,j-1) + \sigma_u n(i,j) \quad \forall i,j \in I,J \quad (1)$$

where i,j is the scene pixel location, $n(i,j)$ is a zero mean, unit variance, random sequence, $\{C_1, C_2, C_3\}$ are the spatial model parameters, and σ_u is the standard

deviation of the driving process. A reflectance array $R(i,j,\lambda)$, is then created with Eq. 2,

$$R(i,j,\lambda) = \rho_k(\lambda) + \sigma_k(\lambda)s(i,j) \quad \forall i,j \in I,J; \lambda \in \Lambda \quad (2)$$

where the appropriate class reflectance data are used within boundaries B_k . The spectral radiance is then calculated with Eq. 3,

$$L_\lambda(iG,jG) = \{[(1/\pi)E_{\lambda,sun}(S) + L_{\lambda,sky}(S)]R_k(i,j,\lambda) T_{\lambda,atm}(S) + L_{\lambda,path}(S)\} \quad \forall i,j \in I,J \quad (3)$$

where S is the set $\{\theta_{sun}, \phi_{sun}, \theta_{sensor}, \phi_{sensor}, a, V_\eta\}$ of goniometric and atmospheric parameters. $E_{\lambda,sun}$ is the solar spectral irradiance at the surface, $L_{\lambda,sky}$ is the skylight spectral radiance, $T_{\lambda,atm}$ is the atmospheric transmittance, and $L_{\lambda,path}$ is the path spectral radiance.

4. SENSOR MODEL

The sensor model transforms the scene spectral radiance file into a multispectral digital image of the scene. The model first applies the spectral response by integrating each band's spectral response across the scene spectral range, then applies the spatial response of the sensor by the discrete convolution of separable line spread functions in the two spatial dimensions. Next, noise is added to the resulting image before the channel gain is applied and the final conversion to quantized levels occurs based on the number of radiometric bits. Table 2 shows the sensor model parameters.

<u>Sensor Parameters</u>	<u>Symbol</u>
Altitude	H
Cross-track line spread function	$h_x()$
Along-track line spread function	$h_y()$
Cross-track sampling interval	X
Along-track sampling interval	Y
Number of spectral channels	L
Channel spectral response	$s_l(\lambda)$
Maximum channel gain	gain _l
Shot noise level (std. deviation)	$\sigma_s(l)$
Thermal noise level (std. deviation)	$\sigma_t(l)$
Calibration error (std. deviation)	$\sigma_c(l)$
Number of radiometric bits	Q

Table 2. Sensor Model parameters

Mathematically, the sensor model can be described as follows. The resulting array after the spatial and spectral responses are applied, $y(m,n,l)$, is computed as in Eq. 4,

$$y(m,n,l) = \frac{1}{XY} \sum_{\Lambda} \sum_J \sum_I L_\lambda(iG,jG) h_x(mX-iG) \cdot h_y(nY-jG) G^2 s_l(\lambda) \Delta_\lambda \quad (4)$$

where m,n are pixel locations in the multispectral image, λ is the wavelength index of the scene file, and l is the channel index of the image. Noise is then applied by the use of random number generators, n_1, n_2 , which are zero mean unit variance Gaussian, and u which is uniform $(-0.5,+0.5)$, and the appropriate standard deviation multipliers to produce the noisy image $z(m,n,l)$, as in Eq. 5,

$$z(m,n,l) = [\sigma_t(l)n_1(m,n) + y(m,n,l) + \sigma_s(l)n_2(m,n)y(m,n,l)] \cdot [1 + \sigma_c(l)u(m,n)] \quad (5)$$

Finally, the channel gain is applied and A/D occurs as in Eq. 6,

$$d(m,n,l) = [z(m,n,l)/\text{gain}] \cdot (2^Q - 1) \quad (6)$$

and the multispectral image $d(m,n,l)$ is obtained.

This model is extremely flexible as any spatial and spectral response can be used since they are defined by arrays. Also, different noise mechanisms may be simply inserted into the signal chain as they may be identified.

5. PROCESSING MODEL

The task of the processing portion of the simulator is to take the multispectral image from the sensor, and any other user defined input data and then compute an output measure, eg., classification accuracy. At present, the model used in the simulation uses user defined training areas and a Gaussian maximum likelihood classifier to classify each pixel in the image. The only parameter available here is the percentage of training area pixels. Since the user defined the original scene, a classification accuracy can be computed directly.

This model may be enhanced by the inclusion of feature extraction algorithms before the classification stage, or by the addition of alternative classification methods.

6. RESULTS

For the results that follow a standard scene, sensor, and processing definition was established. The scene was a 150x150 area of 10 meter pixels containing four small grain classes (rye, barley, wheat, and triticale), over a spectral range of 0.4 to 1.1 μm in 10 nm intervals with a rural atmosphere of 5 km meteorological range. The sensor was an abbreviated spectral band (first four bands) version of the Landsat Thematic Mapper instrument. Measured spectral (Ref. 1) and spatial responses (Ref. 4), and noise parameters (Ref. 5) were used. Radiometric resolution was set at 8 bits. The spatial response of TM is such that the image file was then 50x50 pixels. Figure 2 shows the spatial arrangement of the spectral classes in the scene and the training areas selected.

The first experiment illustrates the effect due to nonvertical sensors, and illumination angle. While one was varying, the other was held at 0° zenith angle. The result is shown in Figure 3.

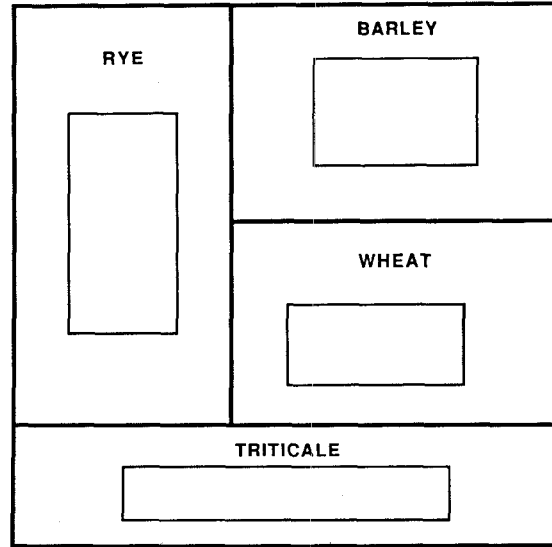


Figure 2. Spatial Layout of Classes and Training Areas

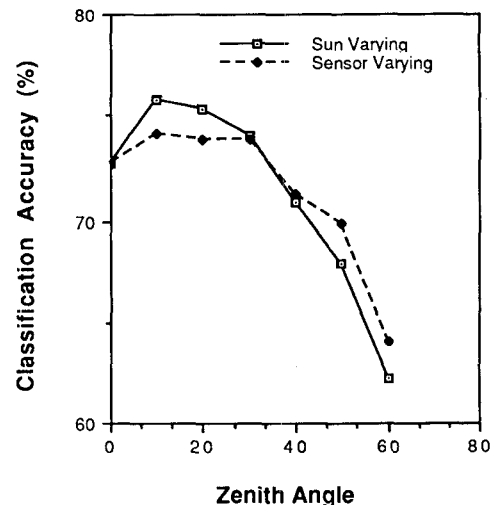


Figure 3. Goniometric Effects

The accuracies of classification of the four classes were averaged to obtain the overall accuracy, and five simulation runs were averaged to obtain these results. Note that these results were obtained without accounting for the non-Lambertian surface reflectance characteristics. Since the surface reflectance didn't change with angle in this experiment, the variation in the results most likely came from the effect of the atmosphere. These results took about 75 minutes of CPU time on a superminicomputer running at about 20 MIPS.

Another experiment was performed to illustrate how the effect of the atmosphere relates to sun angle. For this experiment the sensor was again the abbreviated band Landsat Thematic Mapper at 0° zenith angle. Figure 4 shows the result.

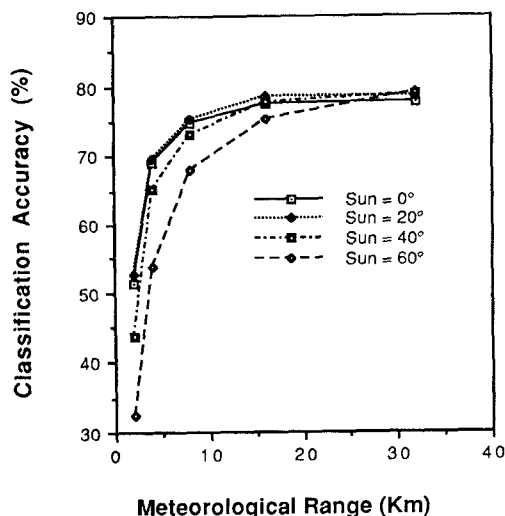


Figure 4. Effect of Atmosphere for Varying Sun Angles

From this result, it can be seen that the angle of the sun has a greater effect on classification accuracy in a hazy atmosphere.

Next, an experiment was performed to see how the radiometric resolution affected classification accuracy for various types of sensors. In addition to the Landsat TM sensor used above, also used were the Landsat MSS, SPOT MSS, and a high spectral resolution (61 channels from 0.4 μm to 1.0 μm) sensor (HIVNIR) with the spatial resolution of Landsat TM. Figure 5 shows the results using a 10 km meteorological range.

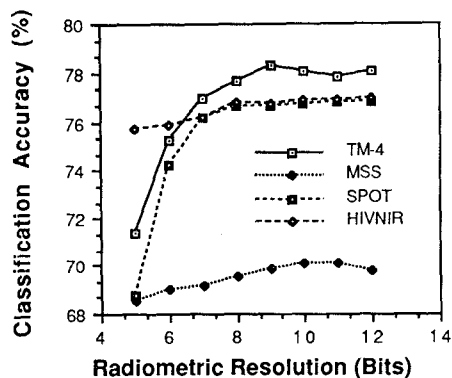


Figure 5. Radiometric Resolution for Various Sensors

Here it appears that accuracy doesn't improve significantly at radiometric resolutions greater than 7 or 8 bits. In addition to the spatial and spectral band differences, the absolute level of classification accuracy for the various sensors may be related to the S/N ratios used in the simulation.

7. CONCLUSIONS

We have presented some initial results of applying a remote sensing system simulation to varying system configurations. While these results may indicate trends resulting from changing the system parameters, their veracity should not be accepted in the absolute. It must be stressed that these results are for a particular system model. Hopefully, they do illuminate relationships among the parameters and illustrate the potential applications of such detailed simulations.

8. REFERENCES

- Huck, F.O., R.E. Davis, C.L. Fales, R.M. Aherron, R.F. Arduini, and R.W. Samms, "Study of Remote Sensor Spectral Responses and Data Processing Algorithms for Feature Classification," *Optical Engineering*, vol. 23, no. 5, pp. 650-666, September/October 1984.
- Kerekes, J.P. and D.A. Landgrebe, "A Noise Taxonomy for Remote Sensing Systems," in *Proceedings of IGARSS '87*, pp. 903-908, Ann Arbor, MI, 18-21 May, 1987.
- Kneizys, F.X. et.al., "Atmospheric Transmittance/Radiance Computer Code LOWTRAN 6," AFGL-TR-83-0187, Air Force Geophysical Lab, Bedford, MA.
- Markham, B.L., "The Landsat Sensors' Spatial Responses," *IEEE Transactions on Geoscience and Remote Sensing*, vol. GE-23, No. 6, November 1985, pp 864-875.
- Malaret, E.R., "The Relationship of Sensor Parameters to Applications Data Analysis," Master's Thesis, School of Electrical Engineering, Purdue University, West Lafayette, IN 47907, August 1982.